Authors' accepted manuscript
Paper presented at the IEEE International Conference on Robotics and Automation (ICRA) - Philadelphia, PA, USA, May 23-27, 2022
Final published version will be available at https://ieeexplore.ieee.org/xpl/conhome/1000639/all-proceedings

Design and Modeling of a Spherical Robot Actuated by a Cylindrical Drive*

Bruno Belzile[1] and David St-Onge[1]

***Abstract*— Rolling spherical robots have been studied in the past few years as an alternative to legged and wheeled robots in unstructured environments. These systems are of uttermost interest for space exploration: fast, robust to collision and able to handle various terrain topologies. This paper introduces a novel barycentric spherical robot, dubbed the Autonomous Robotic Intelligent Explorer Sphere (ARIES). Equipped with an actuated cylindrical joint acting as a pendulum with two degrees-of-freedom (DoF), the ARIES has a continuous differential transmission to allow simultaneous rolling and steering. This mechanism allows an unprecedented mass allocation optimization, notably to provide a low center of mass. Kinematics and dynamics of this novel system are detailed. An analysis of the steering mechanism proves that it is more efficient than a more conventional 2-DoF tilting mechanism, while also retaining more space for a payload, for instance to host sensors for simultaneous localization and mapping, in the upper part of the sphere. Moreover, the kinematic input/output equations obtained significantly simplify the device's control. Finally, we present a first complete prototype with preliminary experimental tests.**

I. Introduction

Alternatives to traditional wheeled robots have been studied for space exploration, as they are not necessarily adapted for the challenging terrain topology that can be found on the Moon and on Mars. Instead of relying on a single highly agile platform (i.e. legged robot), our approach suggests the use of several spherical rolling robots dropped near a targeted area by a lander unit to explore it. The spherical shape of the robot grants it good maneuverability and is well suited to protect its internal equipment (sensors and computer) and actuators from potential collisions as well as to seal it off from the harsh exterior environment.

A large range of spherical robots can be found in the literature for various applications, ranging from child-development studies [1] to underwater exploration [2] and agriculture [3]. Some are also commercially available, commonly sold as toys to learn robotics [4].

While there are as many spherical rolling robot designs as there are specific sets of characteristics, their locomotion systems can be summarized in three broad categories: 1) barycentric [5], [6], [7], [8], [9]; 2) conservation of the angular momentum [10], [11], [12], [13], [14]; and 3) shell deformation [15]. In this paper, only robots with internal actuation systems are considered, as oppose to spherical robots using outer forces, such as the NASA/JPL Tumbleweed polar rover [16].

Fig. 1. Autonomous Robotic Intelligent Explorer Sphere (ARIES), with a diameter of 40 cm

Barycentric spherical robots (BSR) are by far the most common kind [17]. To drive the rolling motion, the center of mass (CoM) of the robot is moved away from the center of rotation (CoR). They can be classified in several subcategories. First, pendulum-based BSRs, in which the pendulum bob points in the direction of desired travel, are fairly common. While only one bob is necessary, Li, Deng and Liu proposed a BSR with two [18] and DeJong et al., four [9], to increase their maneuverability, at the expense of more complex control schemes. To steer its BSR, Schroll [19] designed and patented a differential mechanism to tilt the bob in a direction orthogonal to the rolling motion. Second, some researchers have also built prototypes with a smaller wheeled robot inside the sphere [20] or with an internal drive unit (IDU) [21], [20], [22]. However, these systems are known to suffer from slipping [17]. Finally, some BSRs use sliding masses to control the location of the CoM [23], [24], [25]. They are generally more difficult to control than the two other subcategories described above. Similarly, Tafrishi et al. proposed using masses moving inside pipes filled with fluid to control the location of the CoM, thus generating motion [26].

In this paper, a pendulum-based barycentric spherical robot is proposed. To be able to steer the device, nicknamed the Autonomous Robotic Intelligent Explorer Sphere (ARIES)[1], depicted in Fig. 1, we designed a novel differential mechanism based on the concept of the actuated cylindrical joint. The main advantages of our concept is that we obtain a more robust internal mechanism, we optimize the mass

*This work was supported by NSERC Discovery Grant (RGPIN-2020-06121) and the Canadian Space Agency (CSA-FAST 19FAPOLA32).

[1]École de technologie supérieure, Montréal, Department of Mechanical Engineering, bruno.belzile.1@ens.etsmtl.ca, david.st-onge@etsmtl.ca

[1]patent pending

allocation (no dead weight), we provide a really low CoM and we have a nearly completely empty upper half of the sphere, which is ideal to house a payload. Moreover, as this paper will show, the 2-degrees-of-freedom (DoF) output of the cylindrical joint can be computed with a linear combination of the motors' angular position and the curvature radius while steering is inversely proportional to the linear displacement of the cylindrical joint. This two elements greatly simplify the control of the ARIES. In the sequel, the governing principle of the proposed differential drive is explained. Then, the kinematics and dynamics are detailed alongside a comparison with a more conventional tilting mechanism. Finally, we present a prototype of the ARIES as well as some preliminary experiments.

II. Barycentric Spherical Robot with a Cylindrical Drive

To be able to generate the rolling motion and steer a barycentric spherical robot, the CoM must be able to move in at least two directions relative to the outer shell. The idea behind ARIES is to control the position of the CoM over a virtual cylinder located inside the sphere. The center of the latter is located on the axis of the former. To obtain this type of motion of the CoM, a cylindrical actuated joint is needed: a differential mechanism with two DoFs, a rotation and a translation, about the same axis (in our case passing through the center of the sphere). Harada et al. designed one example of this kind of mechanisms, dubbed the C-drive, with a RHHR[2] kinematic chain [27]. Karimi, Eskandary and Angeles later improved the device with belts and pulleys shaped into a translating Π-joint [28] that was used to drive a two-limb isostatic pick-and-place robot [29].

Inspired by this work, our design, shown in Fig. 2, transforms the concept into a novel implementation. In both applications, two identical revolute motors are used to reduce the complexity and two lead screws with the same pitch, one righthand, the other lefthand, support the linear motion. In their implementation, Karimi, Eskandary and Angeles attached the motors of the C-drive to the base and the output shaft was connected to the proximal link of a manipulator. In our approach however, the motors are rigidly attached to the mobile platform (pendulum), as shown in Fig. 3. Therefore, in our application, the motors are moving inside the spherical shell by translating about the rolling axis of the robot, as depicted in Fig. 3. The output of this cylindrical drive generates the rotation required for the sphere to roll plus the translation needed for it to steer. The mechanical concept was fundamentally redesigned for this different output as well as to minimize its mass.

As can be seen in Figs. 2 and 3, the three pulleys are on the same plane, the latter passing through the center of the sphere. The upper pulley, i.e. the output of the cylindrical drive, is rigidly attached to the rolling axis of the sphere. The two motors are rigidly attached to the same body,

[2]R, H and C stand for revolute, helical (screw) and cylindrical joint respectively.

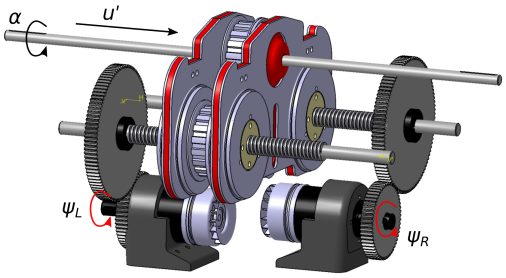

Fig. 2. Rendering of the cylindrical drive only (mobile platform not shown)

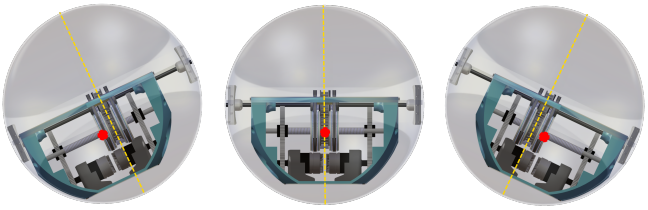

Fig. 3. Steering of the sphere by tilting it with translation of the CoM (illustrated by the red dot, median plane by the dashed yellow line)

the latter translating as a function of the output of the motors. If both motors turn at the same rate in the same direction, they generate a pure rotation about the output shaft; one resulting into a forward-only motion of the sphere. If they turn in opposite direction, again with the same rate, they generate a pure translation. The sphere then tilts in the plane orthogonal to the rolling motion. This motion is limited, as the translation component of the cylindrical drive is physically bounded inside the shell. Any cylindrical motion can be generated by a linear combination of the two foregoing motions.

We define the joint variables[3] of the cylindrical drive (input) as $\boldsymbol{\psi} \equiv \begin{bmatrix}\psi_L & \psi_R\end{bmatrix}^T$. The output of the cylindrical drive, defined by the variables u' and θ, respectively for translation and rotation, is arrayed in the vector $\mathbf{d}$. The matrix relation between the output and the input is derived in the next section.

TABLE I
Parameters and Variables

R	radius of the sphere
r	distance between center of the sphere and CoM of the pendulum
m_s	mass of the shell
m_p	mass of the pendulum
I_s	moment of inertia of the shell
I_p	moment of inertia of the pendulum
θ	rolling angle of the sphere about x-axis of frame $\mathcal{F}_o$
ϕ	rolling angle of the sphere about y-axis of frame $\mathcal{F}_o$
ξ	rolling angle of the sphere about z-axis of frame $\mathcal{F}$
α	rotational output of the cylindrical joint
u'	translational output of the cylindrical joint
u	translation of the CoM of cylindrical pendulum
k_p	mass ratio between the pendulum's translating parts and m_p
p	pitch of the lead screws
G	reduction ratio of the cylindrical joint
g	gravitational acceleration
r_c	curvature radius while steering
$\mathbf{p}_s$	Cartesian position of the center of the sphere in $\mathcal{F}$

[3]Subscripts L and R stand for the left and the right motors.

In the following derivations, we simplify the model. The interactions between rolling motions about the transversal and longitudinal axes are neglected, leading to a decoupled model. Similar decoupled approaches have been applied successfully to wheeled vehicles [30], unicyle/bicycles [31] and other spherical rolling robots [32]. Moreover, considering that a spherical robot generates only one of the two motions (translation for steering, rotation for rolling) at every time step (infinitesimal) is not constraining. Furthermore, the kinetic energy of the tilting motion will be significantly lower than the one related to the rolling motion during simultaneous rolling and steering; thus the decoupled model assumption is adequate.

A. Kinematics

1) Spherical Robot: This section presents the equations relating the translational and angular displacement of the cylindrical drive to the spherical motion. Five frames are required for this derivation: 1) the inertial reference frame $\mathcal{F}$; 2) the frame $\mathcal{F}_o$ that is rotated by the angle ξ about the z-axis of $\mathcal{F}$, where ξ is the heading of the robot; 3) the moving reference frame $\mathcal{F}_m$ attached to the center of the sphere and only allowed to translate with respect to $\mathcal{F}_o$; 4) the frame attached to the center of the shell $\mathcal{F}_s$, with its x-axis aligned with the main rotation axis of the mechanism; 5) the frame attached to the CoM of the pendulum $\mathcal{F}_p$, which is obtained after applying a translation u and a rotation α about the x-axis of $\mathcal{F}_s$ (which is the axis of the cylindrical joint). All five frames are illustrated in Fig. 4. While it is possible to use a generic 3-DoF rotation matrix (i.e. defined from an Euler convention) between $\mathcal{F}_m$ and $\mathcal{F}_s$, our decoupled model allows us to use a single rotation angle at the time. For the rolling motion, the x-axes of $\mathcal{F}_m$ and $\mathcal{F}_s$ are assumed to be parallel. The rotation angle about this shared axis is therefore θ. For the steering/tilting motion, it is y-axes of $\mathcal{F}_m$ and $\mathcal{F}_s$ that are assumed to be parallel, and the angle between their respective x-axes is ϕ. The position of the CoM of the cylindrical pendulum with respect to frame $\mathcal{F}_s$ is

$$ {}^{s}\mathbf{r}_p = \begin{bmatrix} u & r\sin\alpha & -r\cos\alpha \end{bmatrix}^T \tag{1} $$

where r is the distance between the axis of the cylindrical drive and the center of the sphere. Variables u' and α are, respectively, the translational and rotational output of the cylindrical joint, both illustrated in Fig. 2. Because some parts of the cylindrical pendulum do not translate, the translation applied to the CoM of the pendulum is $u = k_p u'$, where k_p, a scalar, is the ratio between the mass that does not translate (eg. the central pulleys) and the total mass of the pendulum.

In order to achieve a decoupled model of the dynamics, velocities corresponding to the forward rolling (subscript r) and steering motions (subscript t) of the robot are separated. Since the angular velocity $\dot{\xi}$ (cf. Fig. 4) can be neglected because it is significantly lower than the other angular velocities, the kinematics and dynamics analyses are conducted with respect to $\mathcal{F}_o$ and not $\mathcal{F}$. Therefore, linear and angular

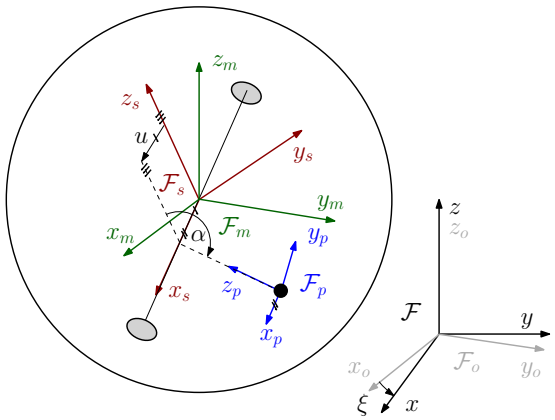

Fig. 4. Frames: $\mathcal{F}$ and $\mathcal{F}_o$ attached to the ground, $\mathcal{F}_m$ and $\mathcal{F}_s$ attached to the center of the sphere, $\mathcal{F}_p$ attached to the CoM of the pendulum

velocities of the shell, respectively $\mathbf{v}_s$ and $\boldsymbol{\omega}_s$, in $\mathcal{F}_o$, are

$$ {}^{o}_{r}\mathbf{v}_s = \begin{bmatrix} 0 & R\dot{\theta} & 0 \end{bmatrix}^T, \quad {}^{o}_{r}\boldsymbol{\omega}_s = \begin{bmatrix} \dot{\theta} & 0 & 0 \end{bmatrix}^T \tag{2a} $$

$$ {}^{o}_{t}\mathbf{v}_s = \begin{bmatrix} R\dot{\phi} & 0 & 0 \end{bmatrix}^T, \quad {}^{o}_{t}\boldsymbol{\omega}_s = \begin{bmatrix} 0 & \dot{\phi} & 0 \end{bmatrix}^T \tag{2b} $$

where R, θ and ϕ are the radius of the sphere, its rolling angle and its tilting angle, respectively. Similarly, expression (1) can be split in

$$ {}^{s}_{r}\mathbf{r}_p = \begin{bmatrix} 0 & r\sin\alpha & -r\cos\alpha \end{bmatrix}^T \tag{3a} $$

$$ {}^{s}_{t}\mathbf{r}_p = \begin{bmatrix} u & 0 & -r \end{bmatrix}^T \tag{3b} $$

The angular velocity of the pendulum, i.e. the cylindrical drive, defined in $\mathcal{F}_s$, is

$$ {}^{s}_{r}\boldsymbol{\omega}_p = \begin{bmatrix} \dot{\alpha} & 0 & 0 \end{bmatrix}^T \tag{4} $$

and then in frame $\mathcal{F}_m$

$$ \begin{aligned} {}^{m}_{r}\boldsymbol{\omega}_p &= {}^{m}_{r}\boldsymbol{\omega}_s + \mathbf{R}_{x,\theta}\,{}^{s}_{r}\boldsymbol{\omega}_p \\ &= \begin{bmatrix} 0 \\ R\dot{\theta} + r\cos(\alpha-\theta)(\dot{\alpha}-\dot{\theta}) \\ r\sin(\alpha-\theta)(\dot{\alpha}-\dot{\theta}) \end{bmatrix} \end{aligned} \tag{5a} $$

where $\mathbf{R}_{x,\theta}$ is the rotation matrix between frames $\mathcal{F}_s$ and $\mathcal{F}_m$ with respect to the rolling motion. It should be noted that the translational motion of the cylindrical drive used to steer the robot, does not, by definition, generate any angular velocity in $\mathcal{F}_s$. Thus, ${}^{s}_{t}\boldsymbol{\omega}_p$ is equal to the three-dimensional null vector and ${}^{m}_{t}\boldsymbol{\omega}_p$ is equal to ${}^{m}_{t}\boldsymbol{\omega}_s$. Finally, the linear velocity of the pendulum can be computed, in frame $\mathcal{F}_s$, with

$$ \begin{aligned} {}^{o}_{r}\mathbf{v}_p &= {}^{o}_{r}\mathbf{v}_s + {}^{o}_{r}\boldsymbol{\omega}_p \times {}^{o}_{r}\mathbf{r}_p \\ &= {}^{o}_{r}\mathbf{v}_s + {}^{o}_{r}\boldsymbol{\omega}_p \times (\mathbf{R}_{x,\theta}\,{}^{s}_{r}\mathbf{r}_p) \\ &= \begin{bmatrix} 0 \\ R\dot{\theta} + r\cos(\alpha-\theta)(\dot{\alpha}-\dot{\theta}) \\ r\sin(\alpha-\theta)(\dot{\alpha}-\dot{\theta}) \end{bmatrix} \end{aligned} \tag{6a} $$

and

$$ \begin{aligned} {}^{o}_{t}\mathbf{v}_p &= {}^{o}_{t}\mathbf{v}_s + {}^{o}_{t}\mathbf{v}_{p/s} + {}^{o}_{t}\mathbf{v}_p + {}^{o}_{t}\boldsymbol{\omega}_p \times {}^{o}_{t}\mathbf{r}_p \\ &= {}^{o}_{t}\mathbf{v}_s + \mathbf{R}_{y,\phi}\,{}^{s}_{t}\mathbf{v}_{p/s} + {}^{o}_{t}\boldsymbol{\omega}_p \times (\mathbf{R}_{y,\phi}\,{}^{s}_{t}\mathbf{r}_p) \\ &= \begin{bmatrix} R\dot{\phi} - u\sin\phi\dot{\phi} - \dot{\phi}r\cos\phi + \dot{u}\cos\phi \\ 0 \\ -u\dot{\phi}\cos\phi + \dot{\phi}r\sin\phi - \dot{u}\sin\phi \end{bmatrix} \end{aligned} \tag{7a} $$

where $\mathbf{R}_{y,\phi}$ is the rotation matrix between the same frames with respect to the steering/tilting motion.

2) Cylindrical Joint: As mentioned above, the pulleys can only rotate about their axis, but cannot translate inside the sphere. Vector $\mathbf{d}$, the output of the cylindrical joint, is mapped by the (2×2) Jacobian matrix $\mathbf{J}_p$ into the joint variables $\boldsymbol{\psi}$:

$$\boldsymbol{\psi} = \mathbf{J}_p \mathbf{d} \tag{8a}$$

with

$$\mathbf{J}_p \equiv \frac{1}{p} \begin{bmatrix} 2\pi/k_p & p\ G \\ -2\pi/k_p & p\ G \end{bmatrix}, \quad \mathbf{d} = [u \quad \alpha]^T \tag{8b}$$

where u and α, as mentioned above, are the translational and rotational output of the cylindical joint, G and p are, respectively, the gear-reduction ratio of the mechanism and the pitch of the lead screws (taken as the same for symmetry). The ARIES has two independent control variables: the rotation and the translation of the pendulum corresponding respectively to the rolling and the steering motion of the sphere.

B. Dynamics

With the kinematics of the robot, we can now derive its decoupled dynamics model. We refer the reader to the work of Kayacan et al. [32] for the underlying assumptions and their validity. Similarly to other spherical rolling robots, we chose a decoupled approach to simplify the highly nonlinear dynamics of the system. First, some common assumptions are required to formulate the dynamics model with a pendulum, i.e. the system is rolling, without slipping, over a perfectly horizontal surface and the internal dynamics of the actuated cylindrical joint can be neglected with respect to the resulting forces and torques. The Lagrangian approach is chosen to obtain the equations of motion. The decoupled expressions of the kinetic energy are

$$\begin{aligned} K_r =& \frac{1}{2}(m_s ||{}^o_r\mathbf{v}_s||^2 + {}_rI_s ||{}^o_r\boldsymbol{\omega}_s||^2 \\ &+ m_p ||{}^o_r\mathbf{v}_p||^2 + {}_rI_p ||{}^o_r\boldsymbol{\omega}_p||^2) \end{aligned} \tag{9a}$$

$$K_t = \frac{1}{2}(m_s ||{}^o_t\mathbf{v}_s||^2 + ({}_tI_s + {}_tI_p) ||{}^o_t\boldsymbol{\omega}_s||^2 + m_p ||{}^o_t\mathbf{v}_p||^2) \tag{9b}$$

where ${}_rI_s$ and I_p are, respectively, the moment of inertia of the shell and the pendulum with respect to the plane parallel to the pulleys and passing through the center of the sphere.

With the CoM of the shell located at the geometrical center of the sphere (no effect), the decoupled expression of the potential energy are

$${}_rE_p = -m_p g r \cos(\alpha - \theta) \tag{10a}$$

$${}_tE_p = -m_p g u \sin\phi - r\cos\phi \tag{10b}$$

From E_k and E_p, two decoupled Langragian functions are obtained: L_r with only rotational terms about the transversal axis, and L_t about the longitudinal axis.

For translation along the y-axis of frame $\mathcal{F}_m$, i.e. the forward rolling motion, the Euler-Lagrangian equations are therefore

$$\frac{d}{dt}\left(\frac{\partial L_r}{\partial \dot{\theta}}\right) - \frac{\partial L_r}{\partial \theta} = \tau_\theta, \quad \frac{d}{dt}\left(\frac{\partial L_r}{\partial \dot{\alpha}}\right) - \frac{\partial L_r}{\partial \alpha} = \tau_\alpha \tag{11}$$

It should be noted here that $\tau_\theta = \tau_\alpha = \tau$ is the torque component of the output of the cylindrical joint. When a torque is applied on the sphere, a reaction torque to the pendulum axis occurs in the opposite direction [33]. For translation along the x-axis of frame $\mathcal{F}_m$, i.e. the tilting/steering motion, the Euler-Lagrangian equations are

$$\frac{d}{dt}\left(\frac{\partial L_t}{\partial \dot{\phi}}\right) - \frac{\partial L_t}{\partial \phi} = 0, \quad \frac{d}{dt}\left(\frac{\partial L_t}{\partial \dot{u}}\right) - \frac{\partial L_t}{\partial u} = f \tag{12}$$

where f is the force output of the cylindrical joint. The last four equations can be written in matrix form:

$$\mathbf{M}(\mathbf{q}(t))\ddot{\mathbf{q}}(t) + \mathbf{V}(\mathbf{q}(t), \quad \dot{\mathbf{q}}(t)) = \mathbf{f}(t) \tag{13a}$$

with

$$\mathbf{q} = [\theta \quad \alpha \quad \phi \quad u]^T, \quad \mathbf{f} = [\tau \quad \tau \quad 0 \quad f]^T \tag{13b}$$

where $\mathbf{M}$ is the inertia tensor and $\mathbf{V}$ is an array containing the other wrenches acting on the system, such as internal and external friction forces and the cross-influence of the velocity components (alike coriolis).

C. Curvature Radius

The distance between the cylindrical drive axis and the center of the sphere is r', which, as a function of the pendulum's angle, can be expressed as

$$r' = r\cos(\alpha + \theta) \tag{14}$$

Moreover, regardless of the steering mechanism chosen, the angular velocity of the spherical robot about the vertical axis of the reference frame $\mathcal{F}$ is

$$\Omega = -R\dot{\theta}/r_c \tag{15}$$

where R, $\dot{\theta}$ and r_c are, respectively, the radius of the sphere, the rolling angular velocity of the sphere and the radius of curvature while steering. Therefore, since none of the first two are affected by the steering mechanism, tilting and cylindrical mechanisms must be compare over how the radius of curvature r_c is generated. For the cylindrical pendulum, the magnitude of the friction force between the ground and the sphere is computed with the following expression:

$$\begin{aligned} ||\mathbf{f}_f|| =& ||\mathbf{f}_{c,s}|| + ||\mathbf{f}_{c,p}|| \\ =& m_s r_c \Omega^2 + m_p(r_c + u\cos\phi)\Omega^2 \\ \approx& (m_s + m_p) r_c \Omega^2 \end{aligned} \tag{16}$$

where $\mathbf{f}_{c,i},\ i = \{s, p\}$ are the centrifugal forces acting on the sphere and the pendulum and Ω is the angular velocity of the sphere about the z-axis in $\mathcal{F}$. As can be seen, the translation component of the cylindrical pendulum is neglected, as r_c is assumed significantly larger than u. Then, the magnitude

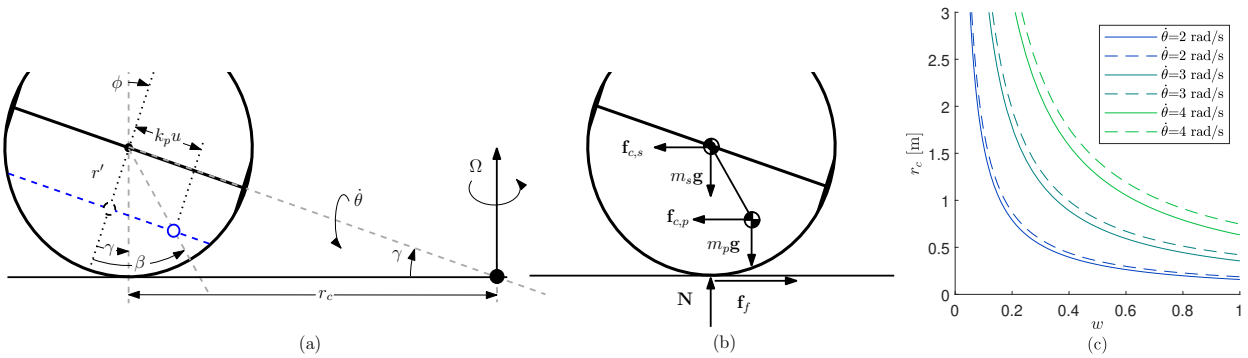

Fig. 5. Steering motion: (a) geometrical model; (b) lateral forces and moments; (c) steering comparison: solid curves for cylindrical pendulum, dashed curves for the tilting pendulum

of the torque acting about the transversal axis of the sphere, i.e. the y-axis of frame $\mathcal{F}_s$, is computed with

$$\begin{aligned} T_y =& -R||\mathbf{f}_f|| - m_p g(r'\sin\phi + u\cos\phi) \\ &+ ||\mathbf{f}_{c,p}||(r'\cos\phi - u\sin\phi) \\ \approx& -R(m_s+m_p)r_c\Omega^2 - m_p g(r'\sin\phi + u\cos\phi) \\ &+ m_p r_c\Omega^2(r'\cos\phi - u\sin\phi) \end{aligned} \tag{17}$$

Knowing that the angular velocity of the sphere, in $\mathcal{F}_m$, is

$$\boldsymbol{\omega} = [-\dot{\theta}\cos\phi \quad -\dot{\phi} \quad \Omega - \dot{\theta}\sin\phi]^T \tag{18}$$

and that its angular momentum is defined as (the moment of inertia of the shell is assumed to be the same regardless of the plane, i.e. ${}_rI_s = {}_tI_s = I_s$)

$$\mathbf{L} = I_s\boldsymbol{\omega} = [-I_s\dot{\theta}\cos\phi \quad -I_s\dot{\phi} \quad I_s(\Omega - \dot{\theta}\sin\phi)]^T \tag{19}$$

then the total torque applied on the sphere, which is the time derivative of $\mathbf{L}$, can also be obtained as $\mathbf{L} = \boldsymbol{\Omega} \times \mathbf{L}$ since the sphere is undergoing uniform circular motion[4], i.e.

$$\mathbf{T} = [I_s\Omega\dot{\phi} \quad -I_s\Omega\dot{\theta}\cos\phi \quad 0]^T \tag{20}$$

Therefore, the second component of $\mathbf{T}$ must be equal to T_y. After some simplifications and using a small-angle assumption for ϕ, we obtain

$$r_{c,cyl} \approx \frac{-m_p r' R^2\dot{\theta}^2 + I_s R\dot{\theta}^2 + R^3(m_s+m_p)\dot{\theta}^2}{u m_p g} \tag{21}$$

III. Comparison: Tilting vs Translating

Using the same set of parameters (mass, moment of inertia, location of the CoM, etc.), we compare our mechanism with a more conventional 2-DoF tilting mechanism. A pure rolling motion will result in the same behavior, since they are both based on the same principle. However, the steering mechanisms differ: ours generates a translation, while the more conventional 2-DoF tilting mechanism generates a rotation. In both cases, steering is a function of the deviation of the CoM with respect to the center plane of the sphere, as shown in Fig. 5. The original location of the CoM is assumed to be the same for both steering systems.

[4]Here, $\boldsymbol{\Omega}$ is the angular velocity vector defining the uniform circular motion, i.e. $\boldsymbol{\Omega} = [0 \quad 0 \quad \Omega]^T$ and should not be confused with $\boldsymbol{\omega}$.

A. Curvature Radius

The curvature radius r_c is not computed the same way depending on the steering mechanism implemented. As obtained by Kayacan et al. [32], an equivalent expression exists for a 2-DoF tilting pendulum (again assuming that ϕ remains small), i.e.

$$r_{c,tilt} \approx \frac{R\dot{\theta}^2(I_s - m_p R r'\cos\beta) + R^3\dot{\theta}^2(m_s+m_p)}{m_p g r'\sin\beta} \tag{22}$$

We can therefore see that both eqs. (21&22) above have a similar structure, i.e.

$$r_c \approx C(A - B\zeta)/\eta \tag{23}$$

where

$$A = I_s + R^2(m_s+m_p), \quad B = m_p r' R, \quad C = \frac{R\dot{\theta}^2}{m_p g} \tag{24a}$$

$$\zeta_{cyl} = 1, \quad \zeta_{tilt} = \cos\beta, \quad \eta_{cyl} = u, \quad \eta_{tilt} = r'\sin\beta \tag{24b}$$

We can see that the curvature radius is a function of the rolling angular velocity $\dot{\theta}$ and u for the cylindrical mechanism or β for the tilting mechanism. The slower the sphere rolls, the smaller is the curvature radius. We perform a numerical comparison using these parameters values: $I_s = 0.25$ kgm^2, $I_p = 0.2$ kgm^2, $m_s = 1$ kg, $m_p = 5$ kg, $R = 0.2$ m and $r = 0.1$ m. Moreover, since the curvature radius for one mechanism is function of an angle (β) and the other of a length u, the former is normalized with respect to 30° and the latter to 0.058 m (realistic maximum values with regards to the scale of our prototype discussed in the next section), resulting in the variable w. Furthermore, if the cylindrical joint makes a translation of $u = 0.058$, the line between the CoM of the pendulum and the center of the sphere makes an angle of 30° with the z-axis of $\mathcal{F}_p$.

Figure 5(c) shows that the curvature radius is generally smaller with the cylindrical pendulum with respect to w. We can argue that our mechanism performs better regarding the steering motion.

B. Torque

Without the torque from the motors, the cylindrical drive is only statically balanced in three positions: the central

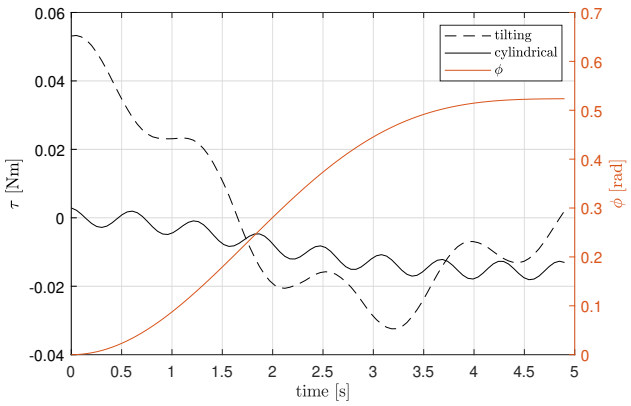

Fig. 6. Torque needed for a typical tilting motion; solid curve for cylindrical pendulum ($\tau = pf$), dashed curves for the tilting pendulum

position $u = 0$ and when it is in contact with its mechanical limits ($u = u_{min} < 0$ or $u = u_{max} > 0$). Indeed, the distance between the center of the sphere and the CoM of the pendulum increases if $|u| > 0$. The conventional tilting mechanism, however, is stable at every value of β. In practice, considering friction and the high gear-reduction ratio of the drive, a stable position exists for any value of u in a real-life scenario. This observation leads to a neat advantage: it reduces the motor torque needed to tilt the robot with a cylindrical drive. The phenomenon is illustrated in Fig. 6, where a similar tilting motion of the sphere ($u = 0.058$ m for the cylindrical drive, $\beta = 30°$ for the 2-DoF tilting mechanism) is conducted with both mechanisms with the dynamics model detailed in Section II-B.

C. Other considerations

There are, however, other advantages for the cylindrical pendulum over the tilting mechanism. For instance, the former leaves the upper part of the sphere mostly empty, which can be useful to host a payload like sensors such as a LiDAR. Moreover, the conventional tilting mechanism requires a lot more internal workspace (empty space for the pendulum motion) than ours. It should also be noted that, as illustrated in Fig. 5(a), the CoM of the pendulum is further away from the center of the sphere with a cylindrical mechanism while steering. Therefore, the maximum torque output of the pendulum is greater.

IV. Prototype and Preliminary Tests

The prototype was shown in Figs. 1&7. As can be seen in the latter, only the cylindrical coupler, highlighted in blue, and the output shaft can translate relative to the mobile platform. Two identical Maxon EC 45 flat 30 W brushless motors with a 26:1 gear are required to power the cylindrical drive.

The curvature radius was determined experimentally to validate the concept of the actuated cylindrical pendulum and the model of the system. As shown in Fig. 8, the experimental data approach the curvature estimated by the model for the tested velocity. The noticeable discrepancies can be explained by friction in the mechanism, assumptions

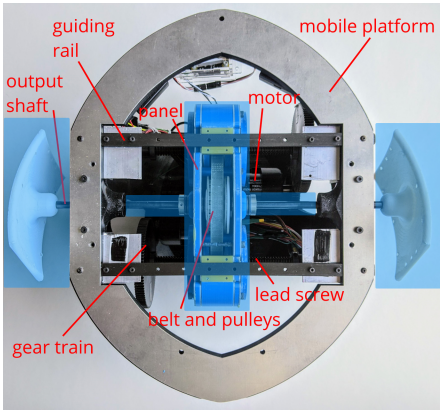

Fig. 7. Inside of the cylindrical drive (all parts that can translate relative to the mobile platform are highlighted in blue)

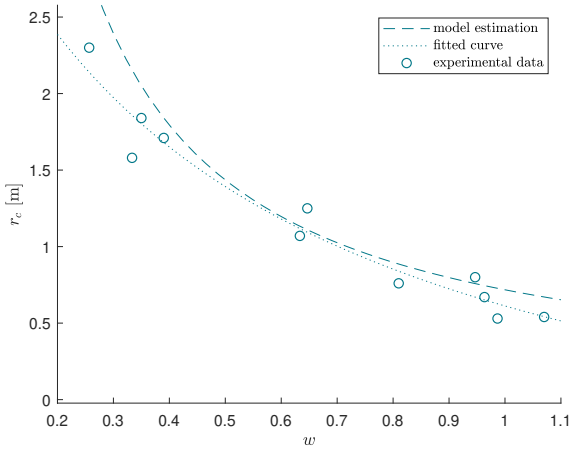

Fig. 8. Experimental curvature radius for $\dot{\theta} = 4.26$ rad/s; dashed curves for estimation from the model, circles for experimental data

made in the model and inertial parameters that do not perfectly fit reality. Nevertheless, this shows that the ARIES can be steered with a relatively small curvature radius at a reasonable speed and that it can be controlled.

V. Conclusion

In this paper, a novel spherical rolling robot driven by a cylindrical actuated joint was proposed. This 2-DoF differential mechanism allows simultaneous rolling and steering with a robust mechanism based only on two identical motors. Kinematics and dynamics of this mechanism were first presented and its characteristics were compared to a more conventional tilting system. The cylindrical pendulum was found to be more efficient than tilting counterparts regarding to steering, while also enabling more free space in the upper half of the sphere for payloads. Moreover, the kinematics and dynamics models show that simple input/output equations can be used to control the robot. A complete design was finally detailed and a prototype was built. Some preliminary experimental data are discussed. Future work will include optimum control, a more thorough experimental validation on various terrains and the analysis of the impact of their topology on the locomotion, as well as the use of the ARIES for simultaneous localization and mapping.

REFERENCES

[1] F. Michaud, J. F. Laplante, H. Larouche, A. Duquette, S. Caron, D. Létourneau, and P. Masson, "Autonomous spherical mobile robot for child-development studies," *IEEE Transactions on Systems, Man, and Cybernetics Part A:Systems and Humans.*, vol. 35, no. 4, pp. 471–480, 2005.

[2] X. Lin and S. Guo, "Development of a spherical underwater robot equipped with multiple vectored water-jet-based thrusters," *Journal of Intelligent and Robotic Systems: Theory and Applications*, vol. 67, no. 3-4, pp. 307–321, 2012.

[3] J. D. Hernández, J. Barrientos, J. Del Cerro, A. Barrientos, and D. Sanz, "Moisture measurement in crops using spherical robots," *Industrial Robot*, vol. 40, no. 1, pp. 59–66, 2013.

[4] A. Wheeler, S. Smith, and D. Gardner, "Using the Sphero BOLT to Engage Students Mathematically," *Journal of Mathematics Education at Teachers College*, vol. 11, no. 2, pp. 55–60, 2020.

[5] B. Zhao, M. Li, H. Yu, H. Hu, and L. Sun, "Dynamics and motion control of a two pendulums driven spherical robot," in *IEEE/RSJ 2010 International Conference on Intelligent Robots and Systems, IROS 2010 - Conference Proceedings*, 2010, pp. 147–153.

[6] Y.-M. Kim, S.-S. Ahn, and Y.-J. Lee, "KisBot: New Spherical Robot with Arms," in *10th WSEAS Int. Conference on Robotics, Control and Manufacturing Technology*, 2010, pp. 63–67.

[7] K. Landa and A. K. Pilat, "Design and start-up of spherical robot with internal pendulum," in *2015 10th International Workshop on Robot Motion and Control, RoMoCo 2015*. Institute of Electrical and Electronics Engineers Inc., 2015, pp. 27–32.

[8] T. J. Ylikorpi, A. J. Halme, and P. J. Forsman, "Dynamic modeling and obstacle-crossing capability of flexible pendulum-driven ball-shaped robots," *Robotics and Autonomous Systems*, vol. 87, pp. 269–280, 2017.

[9] B. P. DeJong, E. Karadogan, K. Yelamarthi, and J. Hasbany, "Design and Analysis of a Four-Pendulum Omnidirectional Spherical Robot," *J Intell Robot Syst*, vol. 86, pp. 3–15, 2017.

[10] S. Bhattacharya and S. K. Agrawal, "Spherical rolling robot: A design and motion planning studies," *IEEE Transactions on Robotics and Automation*, vol. 16, no. 6, pp. 835–839, 2000.

[11] V. A. Joshi and R. N. Banavar, "Motion analysis of a spherical mobile robot," *Robotica*, vol. 27, no. 3, pp. 343–353, 2009.

[12] V. Muralidharan and A. D. Mahindrakar, "Geometric controllability and stabilization of spherical robot dynamics," *IEEE Transactions on Automatic Control*, vol. 60, no. 10, pp. 2762–2767, 2015.

[13] G. C. Schroll, "Dynamic Model of a Spherical Robot from First Principles," Colorado State University, Tech. Rep., 2010.

[14] J. Chen, P. Ye, H. Sun, and Q. Jia, "Design and motion control of a spherical robot with control moment gyroscope," in *2016 3rd International Conference on Systems and Informatics, ICSAI 2016*. Institute of Electrical and Electronics Engineers Inc., 2017, pp. 114–120.

[15] K. W. Wait, P. J. Jackson, and L. S. Smoot, "Self locomotion of a spherical rolling robot using a novel deformable pneumatic method," in *Proceedings of the IEEE International Conference on Robotics and Automation*, 2010, pp. 3757–3762.

[16] A. Behar, F. Carsey, J. Matthews, and J. Jones, "NASA/JPL tumbleweed polar rover," in *IEEE Aerospace Conference Proceedings*, vol. 1, 2004, pp. 388–395.

[17] R. Chase and A. Pandya, "A Review of Active Mechanical Driving Principles of Spherical Robots," *Robotics*, vol. 1, no. 1, pp. 3–23, 2012.

[18] B. Li, Q. Deng, and Z. Liu, "A spherical hopping robot for exploration in complex environments," in *2009 IEEE International Conference on Robotics and Biomimetics, ROBIO 2009*, 2009, pp. 402–407.

[19] G. C. Schroll, "Angular momentum torque enhancement for spherical vehicles," 2009.

[20] J. Alves and J. Dias, "Design and control of a spherical mobile robot," *Proceedings of the Institution of Mechanical Engineers, Part I: Journal of Systems and Control Engineering*, vol. 217, no. 6, pp. 457–467, 2003.

[21] A. Bicchi, A. Balluchi, D. Prattichizzo, and A. Gorelli, "Introducing the 'SPHERICLE': An experimental testbed for research and teaching in nonholonomy," in *Proceedings - IEEE International Conference on Robotics and Automation*, vol. 3. IEEE, 1997, pp. 2620–2625.

[22] Q. Zhan, Y. Cai, and C. Yan, "Design, analysis and experiments of an omni-directional spherical robot," in *Proceedings - IEEE International Conference on Robotics and Automation*, 2011, pp. 4921–4926.

[23] R. Mukherjee, M. A. Minor, and J. T. Pukrushpan, "Simple motion planning strategies for spherobot: a spherical mobile robot," in *Proceedings of the IEEE Conference on Decision and Control*, vol. 3. IEEE, 1999, pp. 2132–2137.

[24] A. H. A. Javadi and P. Mojabi, "Introducing August: A novel strategy for an omnidirectional spherical rolling robot," *Proceedings-IEEE International Conference on Robotics and Automation*, vol. 4, pp. 3527–3533, 2002.

[25] J. Bowkett, M. Burkhardt, and J. W. Burdick, "Combined Energy Harvesting and Control of Moball: A Barycentric Spherical Robot," in *ISER 2016: 2016 International Symposium on Experimental Robotics*. Springer, Cham, 2017, pp. 71–83.

[26] S. A. Tafrishi, M. Svinin, E. Esmaeilzadeh, and M. Yamamoto, "Design, Modeling, and Motion Analysis of a Novel Fluid Actuated Spherical Rolling Robot," *Journal of Mechanisms and Robotics*, vol. 11, no. 4, 2019.

[27] T. Harada, T. Friedlaender, and J. Angeles, "The development of an innovative two-DOF cylindrical drive: Design, analysis and preliminary tests," in *Proceedings - IEEE International Conference on Robotics and Automation*. IEEE, 2014, pp. 6338–6344.

[28] P. Karimi Eskandary and J. Angeles, "The translating Π-joint: Design and applications," *Mechanism and Machine Theory*, vol. 122, pp. 361–370, 2018.

[29] B. Belzile, P. Karimi Eskandary, and J. Angeles, "Workspace Determination and Feedback Control of a Pick-and-Place Parallel Robot: Analysis and Experiments," *IEEE Robotics and Automation Letters*, vol. 5, no. 1, pp. 40–47, 2020.

[30] J. Ackermann and T. Bünte, "Handling Improvement For Robustly Decoupled Car Steering Dynamics," *In Proc. 4TH IEEE Mediterranean Symposium on New Directions in Control and Automation*, 1996.

[31] R. Nakajima, T. Tsubouchi, S. Yuta, and E. Koyanagi, "Development of a new mechanism of an autonomous unicycle," in *IEEE International Conference on Intelligent Robots and Systems*, vol. 2. IEEE, 1997, pp. 906–912.

[32] E. Kayacan, Z. Y. Bayraktaroglu, and W. Saeys, "Modeling and control of a spherical rolling robot: A decoupled dynamics approach," *Robotica*, vol. 30, no. 4, pp. 671–680, 2012.

[33] Y. Ming, D. Zongquan, Y. Xinyi, and Y. Weizhen, "Introducing HIT spherical robot: Dynamic modeling and analysis based on decoupled subsystem," in *2006 IEEE International Conference on Robotics and Biomimetics, ROBIO 2006*, 2006, pp. 181–186.